



Check for updates

RESEARCH ARTICLE

Controllable Growth of Silver Crystallites on the Rear Ag-Si Contact Interface of TOPCon Solar Cells Through an Electrochemical Reduction Reaction Triggered by Laser-Enhanced Contact Optimization

Yongsheng Li¹ | Rui Zhou¹ | Minghan Yu² | Yanhong Tian² | Yuan Lin³ | Feng Pan¹

¹School of Advanced Materials, Peking University, Shenzhen Graduate School, Shenzhen, China | ²National Key Laboratory of Precision Welding & Joining of Materials and Structures, Harbin Institute of Technology, Harbin, China | ³Key Laboratory of Photochemistry, Institute of Chemistry, Chinese Academy of Sciences, Beijing, China

Correspondence: Yanhong Tian (tianyh@hit.edu.cn) | Yuan Lin (linyuan@iccas.ac.cn) | Feng Pan (panfeng@pkusz.edu.cn)

Received: 27 March 2025 | Revised: 18 April 2025 | Accepted: 24 April 2025

Funding: Soft Science Research Project of Guangdong Province, Grant/Award Number: No. 2017B030301013; Guangdong Innovative Team Program, Grant/Award Number: No. 2013N080

Keywords: Ag crystallites | Ag-Si contact | electrochemical reduction reaction | LECO | TOPCon

ABSTRACT

Achieving a balance between passivation and contact has always been crucial for enhancing crystalline silicon (c-Si) solar cells, especially for the currently mainstream N-type TOPCon solar cells. The laser-enhanced contact optimization (LECO) technology improved both the quality and reliability of the front-side Ag–Si contacts in TOPCon solar cells. However, its impact on the rear-side Ag–Si contacts has been overlooked. By investigating LECO, its impact was revealed that electrochemical reduction reaction occurred at the rear-side Ag–Si interface during LECO. This reaction makes it possible for the controlled directional growth of Ag crystallites, thereby optimizing the Ag–Si contact quality. By adjusting the sintering temperature and applying LECO, a balance between passivation and conductivity is achieved, enabling the fabrication of TOPCon solar cells with high open-circuit voltage (V_{oc}) and low series resistor (R_s). This study not only clarifies the role of LECO in optimizing the rear-side Ag–Si contact of TOPCon solar cells but also provides valuable guidance for metallization optimization and power conversion efficiency enhancement of devices.

1 | Introduction

Highly efficient crystalline silicon (c-Si) solar cells with low-cost are essential for achieving the global carbon neutrality goals. The improvement in photoelectric conversion efficiency (PCE) and operation life can dramatically reduce the power generation cost, which has become a vital concern for both research and industrial communities [1]. Tunnel oxide passivated contact c-Si solar cells (TOPCon) have attracted extensive attention owing to their high PCE and low efficiency decay, and they are replacing P-type passivated emitter and rear cells (PERC) quickly. As one of

the mass-produced N-type devices, many challenges remain in constraining their development. One of the major challenges in TOPCon is the high resistance, which poses a significant barrier to efficient carrier extraction. Additionally, recombination of photogenerated carriers at the metal–silicon interface would reduce the overall efficiency [2]. Therefore, regulating the metal–silicon interface to mitigate resistance and recombination remains still an effective strategy for improving TOPCon c-Si solar cells.

To achieve high-quality Ag-Si contacts, process optimization can be tailored based on the device structure. Figure 1a illustrates the

Yongsheng Li and Rui Zhou contributed equally to this study.

© 2025 Wiley-VCH GmbH.

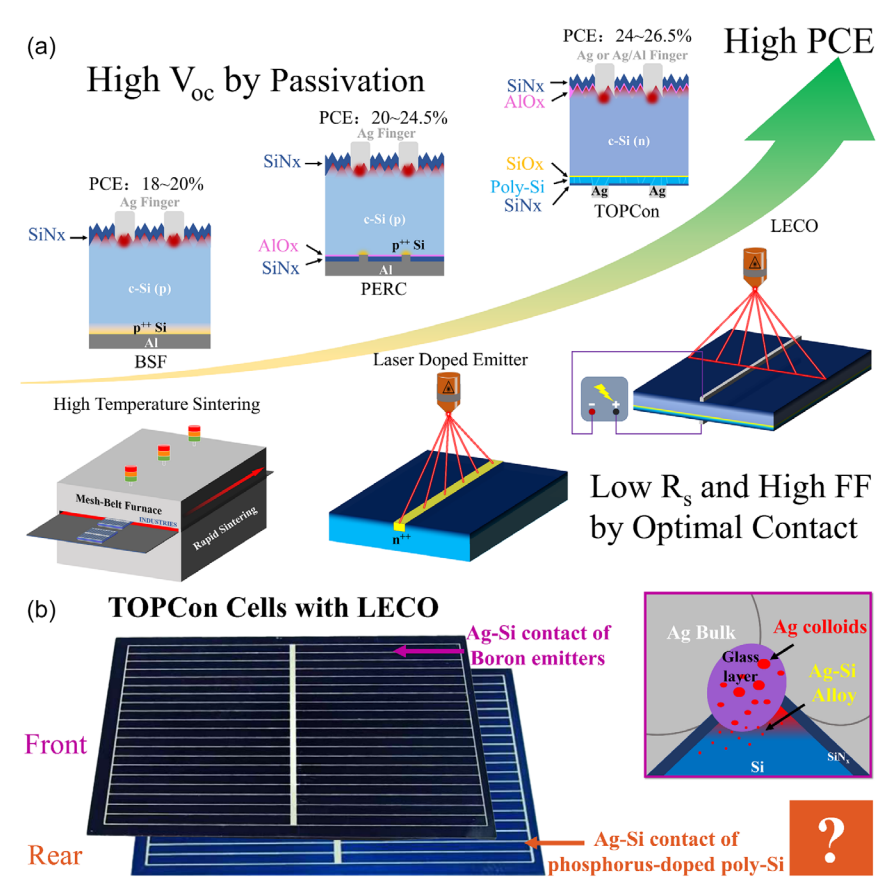


FIGURE 1 (a) The technological evolution of mainstream mass-produced c-Si solar cells; (b) The image of the TOPCon solar cells prepared in this work with its Ag–Si contacts diagrams.

technological evolution of mainstream mass-produced c-Si solar cells. Aluminum back surface field (Al-BSF) solar cells achieved the electrical contact via screen-printed Al paste and Ag pastes with high-temperature co-sintering processes [3]. Since then, thick-film metallic pastes have been widely used in c-Si solar cell manufacturing. Through systematic process optimizations, monocrystalline p-type Al-BSF solar cells had demonstrated a maximum PCE ceiling of 20% [4]. However, the extensive direct Al-Si contact induces substantial carrier recombination losses on the back surface of Si substrate, resulting in relatively low $V_{\rm oc}$ characteristics in Al-BSF solar cells. To enhance passivation efficacy, the PERC architecture was developed by Martin et al. [5] This configuration employed a dual-layer stack of aluminum oxide (Al₂O₃) and silicon nitride (SiN_x) deposited on the rear surface of silicon substrate, enabling superior surface passivation and interfacial modulation. The optimized structure achieved both a $V_{\rm oc}$ of 694 mV and a short circuit current density ($J_{\rm sc}$) of 41.58 mA/cm². Simultaneously, selective emitter (SE) technology was developed to balance excellent passivation with highquality contact performance. By precisely controlling the doping concentration in the contact area through laser doping, only the localized contact region forms a highly doped profile, thereby ensuring optimal contact properties. Consequently, PERC cells had achieved a certified PCE breakthrough of 24.0% in mass production [6]. Building on this foundation, the Fraunhofer Institute for Solar Energy Systems introduced the TOPCon cell technology, marking a significant evolution in c-Si solar cell architecture [7]. This structure enhanced carrier collection efficiency and achieves a higher V_{oc} by utilizing an ultrathin SiO_2 tunneling

layer and doped polysilicon for rear-side passivation. At present, TOPCon solar cells have been gradually becoming mainstream. Concurrently, LECO has been developed to improve the contact quality [8]. By applying an external electric field and laser irradiation, LECO enables the use of Ag paste for the front metallization in TOPCon solar cells, mitigating the carrier recombination issues and the risk of reliability of Ag/Al paste. Although LECO has been implemented in TOPCon production, its underlying mechanisms remain incompletely understood. Recently, many studies proposed mechanisms for the influence of LECO on the Ag-Si contact of the boron emitter on the front side of TOPCon solar cells [8, 9]. Whereas, its impact on the rear Ag-Si contact-often overlooked but critical for device PCE—has yet to be thoroughly investigated. Hence, elucidating these mechanisms is of great significance for improving TOPCon solar cell PCE and advancing this technology.

Our prior investigations revealed that LECO induces localized nano-scale joule heating at the Ag–Si interface, thereby facilitating the formation of Ag–Si alloy on front boron emitters, as shown in Figure 1b [9d].

In this work, we explored the impact of LECO on rear Ag–Si contacts. Laser irradiation generate a high density of charge carriers, and the external reversed electric field drive the carriers flow through the contact interface. In addition to the joule heating effect, this process triggers an electrochemical reduction of Ag⁺ in the glass layer at the interface, forming Ag crystallites that directly contact the poly-Si. So that the contact interface

could be precise controlled. By inhibiting the etching of SiN_x and employing LECO to promote Ag crystallites formation, we achieved nano-scale localized contacts. Consequently, devices with low R_s , high V_oc , and high PCE were obtained.

2 | Experimental Section

2.1 | Materials Synthesis

Preparation of front Ag paste: the front Ag paste was prepared by mixing 89 wt% Ag powders, 2.5 wt% glass frit (primarily consisting of PbO, SiO₂, and B₂O₃, and shown in Figure S1, Supporting Information), 8.5 wt% organic vehicle and using a homogenizer and a three rolls machine to disperse it thoroughly. The rear Ag paste in this work is commercial product, which contains TeO_2 -based glass frit (primarily consisting of TeO_2 , SiO_2 , PbO, and Bi_2O_3).

Front and rear Ag–Si contacts were established on the TOPCon Si wafer (initially a $182 \, \text{mm} \times 182 \, \text{mm}$ commercial Si wafer, laser-cut to dimensions of $53 \times 35 \, \text{mm}$) through screen printing and co-firing in a Despatch CF-SERIES belt furnace. The Ag fingers pattern, a $50 \times 32 \, \text{mm}$ screen-printed layout designed for c-Si solar cells, featuring a single main finger of 0.7 mm width and 21 finer fingers, was utilized for the fabrication of both front and rear electrodes, as depicted in Figure 1b.

The LECO system applied a reverse bias voltage of 15 V, used a laser wavelength of 1064 nm, and operated at a laser power of 20 W (in Figure S2, Supporting Information).

2.2 | Materials Characterizations

The morphology of the materials and devices were examined by scanning electron microscope (SEM, ZEISS SUPRA-55) and elemental distribution was analyzed by energy dispersive spectroscopy (EDS, OXFORD, X-MaxN TSR). Transmission electron microscope (TEM, JEM-3200FS, 300 keV) with EDS (OXFORD, X-max 80) was used to analyze the microstructure and morphology of the Ag–Si contact interface.

2.3 | Device Performance Measurements

The electrical performance of the cells was evaluated under standardized conditions (one sun, illumination with AM 1.5G spectrum, provided by an Abet Technologies Model 11000A Sun 3000 Solar Simulator). The TEM samples were prepared using a focused ion beam (FIB) system from Thermo Fisher (Scios model). Using a calibrated Enlitech PD-QE system with standard Si and Ge photodetectors, the external quantum efficiency and responsivity were recorded. X-ray photoelectron spectroscopy (XPS) tests is conducted on a Thermo Fisher ESCALAB 250X with a monochromatic Al K X-ray source to measure the elements' valence states at contact interface. A RENISHAW inVia Raman Microscope with a 532 nm laser is used to detect structural changes in the glass layer before

and after LECO. The optical image of the rear-side of the TOPCon cell was observed using a LEICA MD2700M.

The graphical parameters of transmission line method (TLM) are shown in Figure S3 (Supporting Information). The R_c was quantified using a Keithley Source-Meter 2602A. The fitted curve can be written as the following equation [10]:

$$Y = A + Bx \tag{1}$$

where x is the distance between adjacent fingers.

 R_c and ρ_c can be calculated according to the following formula:

$$A = 2R_c \tag{2}$$

$$B = \frac{R_{sh}}{W} \tag{3}$$

$$\rho_c = \frac{A^2 W}{4R} \tag{4}$$

where W is the length of finger.

3 | Result

3.1 | The Influence of LECO on Rear Ag-Si Contact

To study LECO influence on rear-side of TOPCon solar cells, we analyzed the rear Ag–Si contacts before and after LECO.

Figure 2a shows the TEM image of the Ag–Si contact prepared at 860°C before LECO. Some inverted triangular Ag spikes emerged on the Ag-Si interface after high-temperature sintering, located

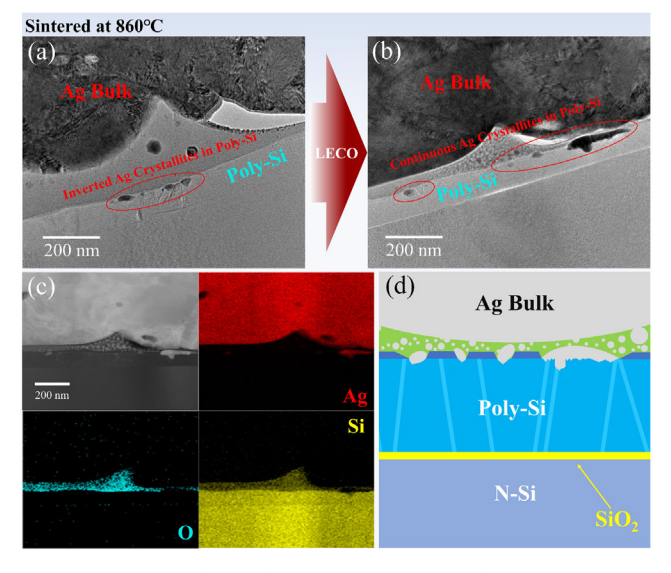


FIGURE 2 | High resolution transmission electron microscope (HRTEM) images of the rear Ag–Si interface of 860°C sample (a) before and (b) after LECO; high angle annular dark field image and element distribution of (c); (d) Schematic diagram of the rear Ag–Si contact structure corresponding to (b).

beneath the glass layer and in direct contact with poly-Si, with a penetration depth of about 30 nm into the poly-Si layer. The TEM image of Ag-Si interface after LECO was shown in Figure 2b. Comparing pre-LECO and post-LECO, the interface morphology changes are evident. On the one hand, the shape of the Ag spikes became irregular after LECO, and their number and size increased significantly (penetration depth up to about 50 nm). On the other hand, more visible Ag colloids emerged within the glass layer. Figure 2c presents the EDS results of the Ag-Si interface after LECO. Through comparison, it can be seen that these large-sized Ag crystallites are located beneath the glass layer and have penetrated into the poly-Si layer. The schematic diagram of the Ag-Si interface structure prepared at 860°C with LECO is shown in Figure 2d. It should be emphasized that due to the different etching rates of Ag on different crystal planes of Si, the Ag crystallites formed by sintering exhibited a regular pyramid shape [11]. In contrast, the Ag crystallites formed by LECO were irregular and differ from by sintering.

Many studies on p-type c-Si solar cells have demonstrated that Ag crystallites can be formed on the surface of the front phosphorus emitter through high-temperature sintering. This direct Ag–Si contact is beneficial for reducing ρ_c . Notably, the phosphorus-doped poly-Si layer on the rear surface of n-type TOPCon cells

is analogous to the structure of the front emitter in p-type c-Si cells, providing a similar condition for carrier contact formation. However, the formation of Ag crystallites through sintering were often difficult to be controlled. The aforementioned experiments indicated that LECO could promote the growth of Ag crystallites. Therefore, we considered utilizing LECO to grow Ag crystallites on interfaces that originally lack them (at lower sintering temperature), in order to obtain an optimal contact interface structure.

Figure $3a_1$ displays the structure of the Ag–Si contact in a cell sintered at 760°C before LECO. From top right to bottom left, the layers are the Ag layer, the glass layer, the SiN_x layer, the poly-Si layer, the ultrathin SiO_2 tunneling layer, and the n-type Si substrate, respectively. Figure $3a_2$ is a partially enlarged view of the Ag–Si contact area marked by the yellow box in Figure $3a_1$. In this region, the etching of SiN_x resulted in direct contact between the Ag colloids-containing glass and poly-Si. Figure $3a_{3-4}$ show the fast Fourier transform (FFT) patterns of different locations in Figure $3a_2$, respectively. The red box corresponds to the Ag colloids in the glass layer, whose face-centered cubic (FCC) structure is clearly distinguishable by its lattice points in the FFT pattern [12]. The green box marks the surrounding glass phase, whose FFT pattern confirms its

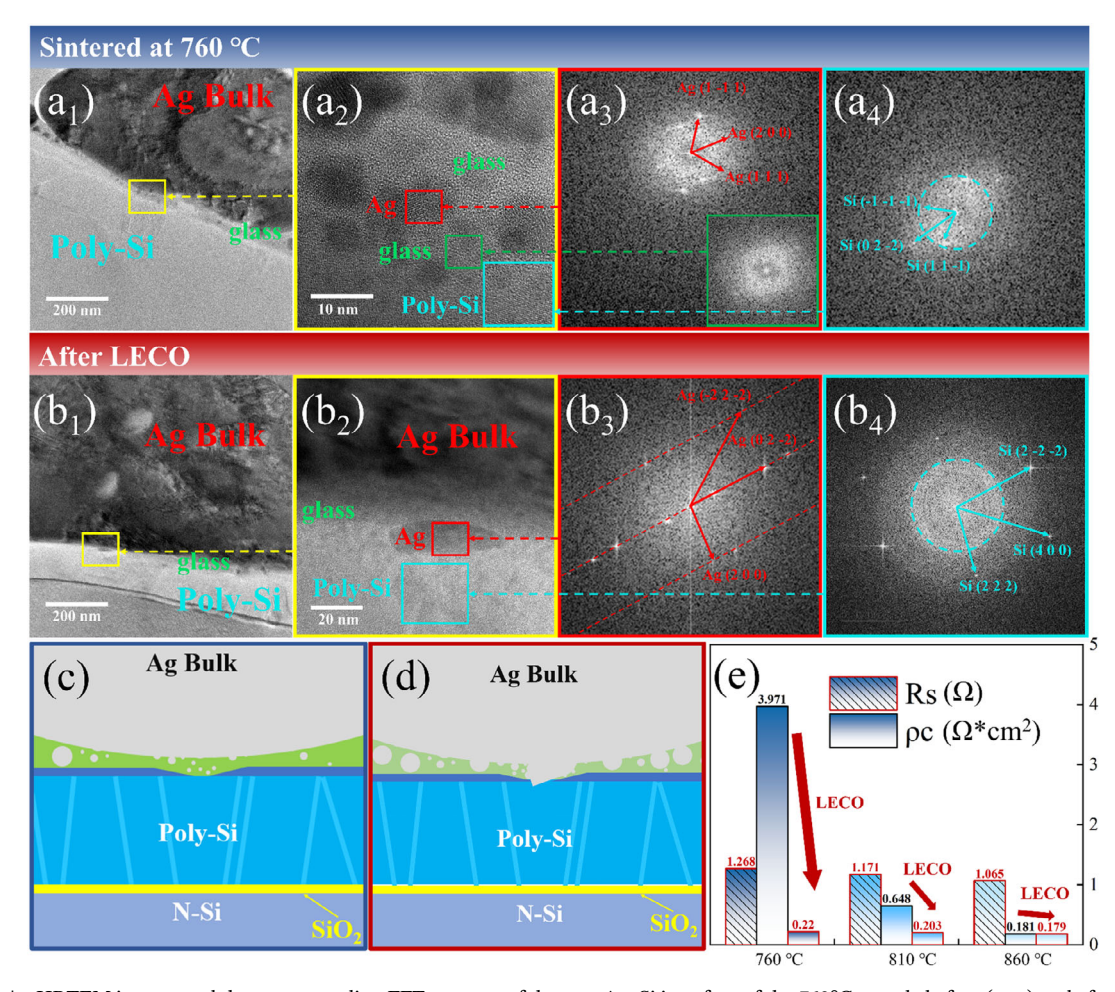


FIGURE 3 | HRTEM images and the corresponding FFT patterns of the rear Ag–Si interface of the 760°C sample before (a_{1-4}) and after (b_{1-4}) LECO; Schematic diagrams of the rear Ag-Si contact structure, with (c) and (d) corresponding to (a) and (b), respectively; (e) R_s of TOPCon cells prepared at different sintering temperatures and the corresponding ρ_c before and after LECO.

amorphous nature. The blue box indicates the poly-Si substrate beneath the glass layer, whose FFT result exhibits a superposition of polycrystalline rings and lattice points, identified as poly-Si [13]. In summary, this rear Ag–Si contact interface of the device was formed via Ag colloids embedded in the glass layer.

The Ag–Si contact structure modified after LECO was shown in Figure $3b_{1-2}$. It can be distinctly observed that a well-defined (approximately 10 nm thick), fan-shaped crystalline structure emerged on the poly-Si layer. Moreover, the number of Ag colloids in the glass layer increased significantly. The FFT pattern of this crystalline structure and he underlying region are presented in Figure $3b_{3-4}$. Based on these results, the red-boxed structure is identified as Ag crystallites, while the material beneath them corresponds to poly-Si. Figure 3c,d illustrate the schematic diagrams of the rear Ag–Si contact structure before and after LECO respectively, for devices fabricated at 760° C. After LECO, Ag crystallites have formed on the surface of poly-Si, establishing direct Ag–Si contacts.

TLM was employed to analyze the changes in ρ_c before and after LECO. Figure 3e displays the $R_{\rm s}$ of TOPCon cells prepared at different temperature and ρ_c of the rear Ag–Si contacts before and after LECO. The $R_{\rm s}$ values of the cells post-LECO are similar, with 1.268, 1.171, and 1.065 Ω at 760°C, 810°C, and 860°C, respectively. For the Ag–Si contact prepared at 760°C without LECO, its ρ_c is 3.971 $\Omega^*{\rm cm}^2$. After LECO, ρ_c decreased to 0.22 $\Omega^*{\rm cm}^2$. In comparison, the ρ_c of the Ag–Si contact at 810°C was halved (reduced by a factor of 2), while the impact of LECO on the ρ_c at 860°C was even more less.

At high-sintering temperatures, despite obvious structural modifications in the Ag-Si interface before and after LECO, the variation in ρ_c remains relatively small. This outcome could be attributed to the Ag crystallites that form direct contact with poly-Si. Various Ag-Si contact models have been proposed, two of which are particularly relevant: direct contact model (Ag and Si form direct contact through Ag crystallites) and tunneling contact model (electrical contact is achieved via Ag colloids within the glass layer) [14]. In practical manufacturing, both types of contacts coexist on the n-type Si side of the Ag-Si interface. Theoretically, increasing Ag colloids in the glass layer can reduce ρ_c [15]. The impact of Ag crystallites on ρ_c is greater than that of Ag colloids [16]. The results in Figure 3 demonstrated that only a minimal quantity of Ag crystallites is required to achieve a significant reduction in rear-side Ag-Si contact resistance, which aligns with previous studies that demonstrated contact formation through the utilization of Ag crystallites.

3.2 | Effects of LECO-Optimized Ag-Si Contacts on TOPCon Solar Cell

Through LECO, a low-density architecture featuring direct poly-Si/Ag bulk contact via Ag crystallites was constructed. This innovation achieved significant optimization of the rear Ag–Si contact, that exerted a substantial influence on device performance. A comprehensive analysis was subsequently conducted to investigate this effect.

Figure 4a presents the J–V curves and V_{oc} of TOPCon cells fabricated at varying sintering peak temperatures after LECO

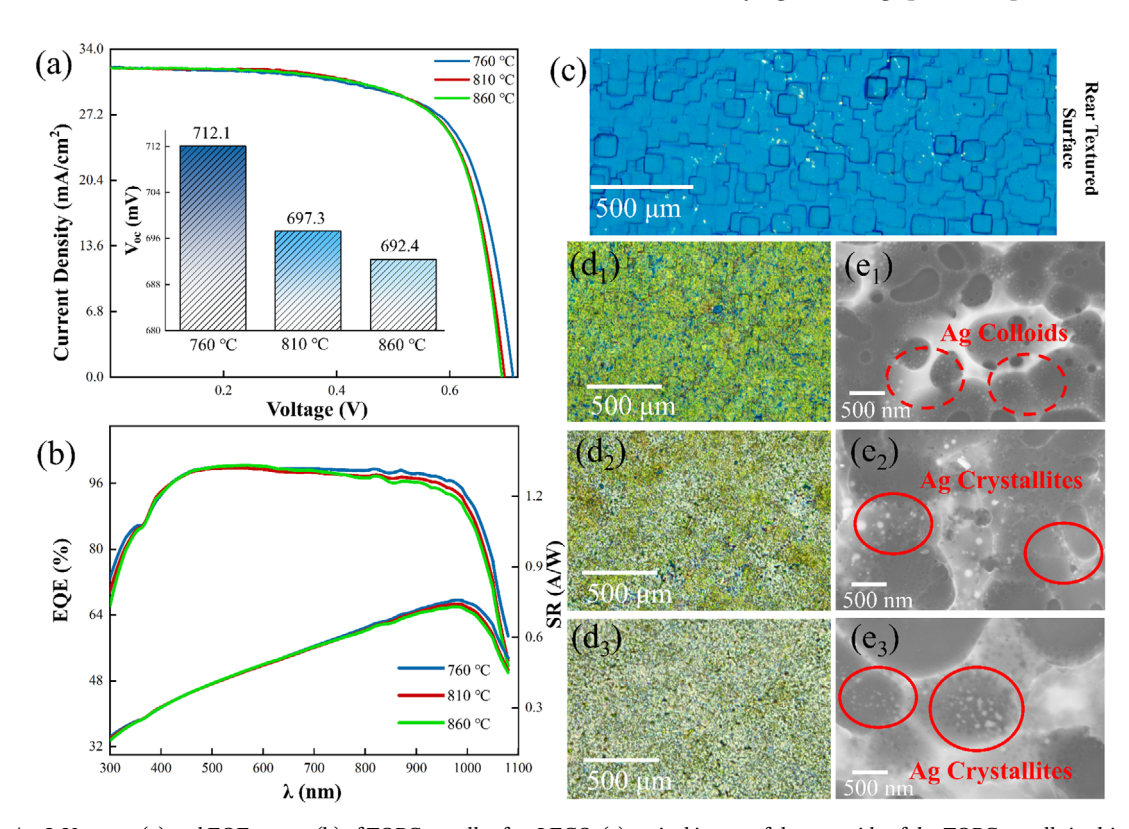


FIGURE 4 | J-V curves (a) and EQE curves (b) of TOPCon cells after LECO; (c) optical image of the rear-side of the TOPCon cells in this work; optical images (d₁₋₃) and SEM images (e₁₋₃) of the metalized regions after removing the rear Ag fingers for devices prepared at 760°C, 810°C, and 860°C without LECO treatment, respectively.

processing, with relevant electrical parameters listed in Table S1 (Supporting Information). The $V_{\rm oc}$ values of cells processed at sintering temperatures of 860°C, 810°C, and 760°C are 692.4, 697.3, and 712.1 mV, respectively. Obviously, V_{oc} increases with decreasing sintering temperature. To investigate the impact of reduced temperature on both front and rear Ag-Si contacts, external quantum efficiency (EOE) testing was conducted (Figure 4b). Analysis of EQE curves reveals that lower sintering temperatures result in a slight increase in EQE in the 300-400 nm wavelength range and a significant enhancement in the 700-1100 nm band. The highest EQE in the long-wavelength region for the 760°C sample indicates reduced back-surface recombination and improved contact quality, which is closely tied to the rear-contact structure [17]. To elucidate the underlying mechanisms, comprehensive characterization of the contact interface from both macroscopic and microscopic perspectives is essential. Figure 4c displays an optical image of the rear-side of a TOPCon cell, featuring a stepped structure covered with a SiN_x layer on its surface. Figure 4d₁₋₃ show optical images of the metalized regions after removing the Ag fingers for devices prepared at 760°C, 810°C, and 860°C, respectively. After dissolving the Ag fingers with HNO₃ and cleaning by ultrasonication, only the glass layer and the blue areas (uncovered or unetched by the molten glass frit) remained on the metalized surface. With increasing sintering temperature, the green glass layer's coverage area expanded continuously, and silvery white reflection regions emerged. On the one hand, higher temperatures enhanced the glass frit's spreading over the silicon nitride layer, promoting etching reactions [18]. This phenomenon can be attributed to the fluidity of the glass frit and the dissolution and reductionprecipitation of Ag within the molten glass frit during rapid sintering process [19]. On the other hand, elevated temperatures increased the solubility of Ag in the molten glass frit, leading to Ag crystallite formation between the glass layer and poly-Si post-etching [19b, 20]. The molten glass frit etched the SiN_x antireflective-coating on the solar cell so that exposing the Si surface, which can be represented by the following reaction equation [21]:

$$4PbO + 2SiN_x \rightarrow 4Pb + 2SiO_2 + xN_2 \tag{5}$$

Then the Ag melted in glass frit could be oxidized and spread to on the exposed Si surface [22]:

$$4Ag + O_2 \rightarrow 2Ag_2O \tag{6}$$

And the oxidized Ag would be reduced to form Ag crystallites [11]:

$$2Ag_2O + Si \rightarrow SiO_2 + 4Ag \tag{7}$$

SEM images reveal the surface micromorphology of the metalized region of the device at varying sintering temperatures, as depicted in Figure $4e_{1-3}$. The regions with light color correspond to the glass layer, while the white nanospheres and irregular block-shaped particles beneath the glass layer are identified as Ag colloids within the glass layer and Ag crystallites beneath the glass layer, respectively. After sintering at 760°C, only a limited number of spherical Ag colloids were observed within the glass layer, with no Ag crystallite formation. When the sintering temperature was increased to 810°C, a small quantity of irregular Ag particles emerged in the glass layer.

Further increasing the sintering temperature to 860°C resulted in an increase in both the size and the number of these irregular Ag particles (crystallites). Based on the optical and SEM morphological results, it is evident that higher sintering temperatures enhance the etching of the SiN_x layer by the glass melt, promoting direct contact between Ag crystallites and poly-Si. However, excessive etching and an overabundance of large Ag crystallites leaded to increased carrier recombination at the interface, thereby reducing the $V_{\rm oc}$ of the solar cells, which aligns with the conclusions of related research [23]. Additionally, the SEM results (in Figure S4, Supporting Information) of contact interface below the front Ag fingers revealed that elevated temperatures similarly enhanced the fluidity of the molten glass frits (of front Ag paste), causing a larger area to be covered and greater etching of the SiN_x by glass layer. It increased carrier recombination at the front contact surface, consistent with the results observed in the shortwavelength region of Figure 4b, so that reduced the $V_{\rm oc}$ of TOPCon solar cells.

By reducing the sintering temperature, the etching of SiN_x was effectively mitigated, which in turn reduced carrier recombination. And the Ag–Si contact optimization via LECO was achieved, leading to decreased contact resistance. Therefore, the TOPCon cell (760°C with LECO) exhibited a low R_s and a high V_oc .

3.3 | The Growth Mechanism of Ag Crystallites by LECO

In Section 3.1 and 3.2, the impact of LECO on Ag–Si contacts is discussed. Then, it is essential to analyze the growth mechanism of Ag crystallites under LECO.

Figure 5a illustrates the LECO process and a schematic representation of the changes that occur in the contact area on the rear-side of the TOPCon solar cells during the LECO treatment. During this process, a reverse voltage was applied to the TOPCon solar cells. Upon laser illumination, abundant electron-hole pairs were generated and separated under reverse bias, with electrons migrating towards the n-poly-Si layer and holes toward the front emitter [24]. Electrons were driven from the n-poly-Si coating on the rear surface toward the Ag fingers, where uneven resistance distribution at the Ag-Si interface causes preferential current flow through low-resistance contact points. Additionally, high-concentration electrons with reducing nature induced Ag aggregation and crystallite growth into the poly-Si layer, thereby reducing the ρ_c of Ag-Si contact on rear side. Figure 5b shows an SEM image of the contact area after Ag finger removal from a TOPCon cell fabricated at 760°C without LECO, featuring a thinner glass layer and no visible Ag colloids/ crystallites. In contrast, LECO-treated cells (Figure 5d) exhibit numerous spherical Ag nanoparticles and irregular crystallites beneath the thinner glass layer. The circular holes above the glass layer in LECO-treated areas correspond to Ag colloids adjacent to the Ag fingers, which are removed during Ag finger lift-off due to lack of glass protection. In regions without these holes, no Ag colloids or Ag crystallites appear beneath glass layer even after LECO, as regions with more Ag colloids

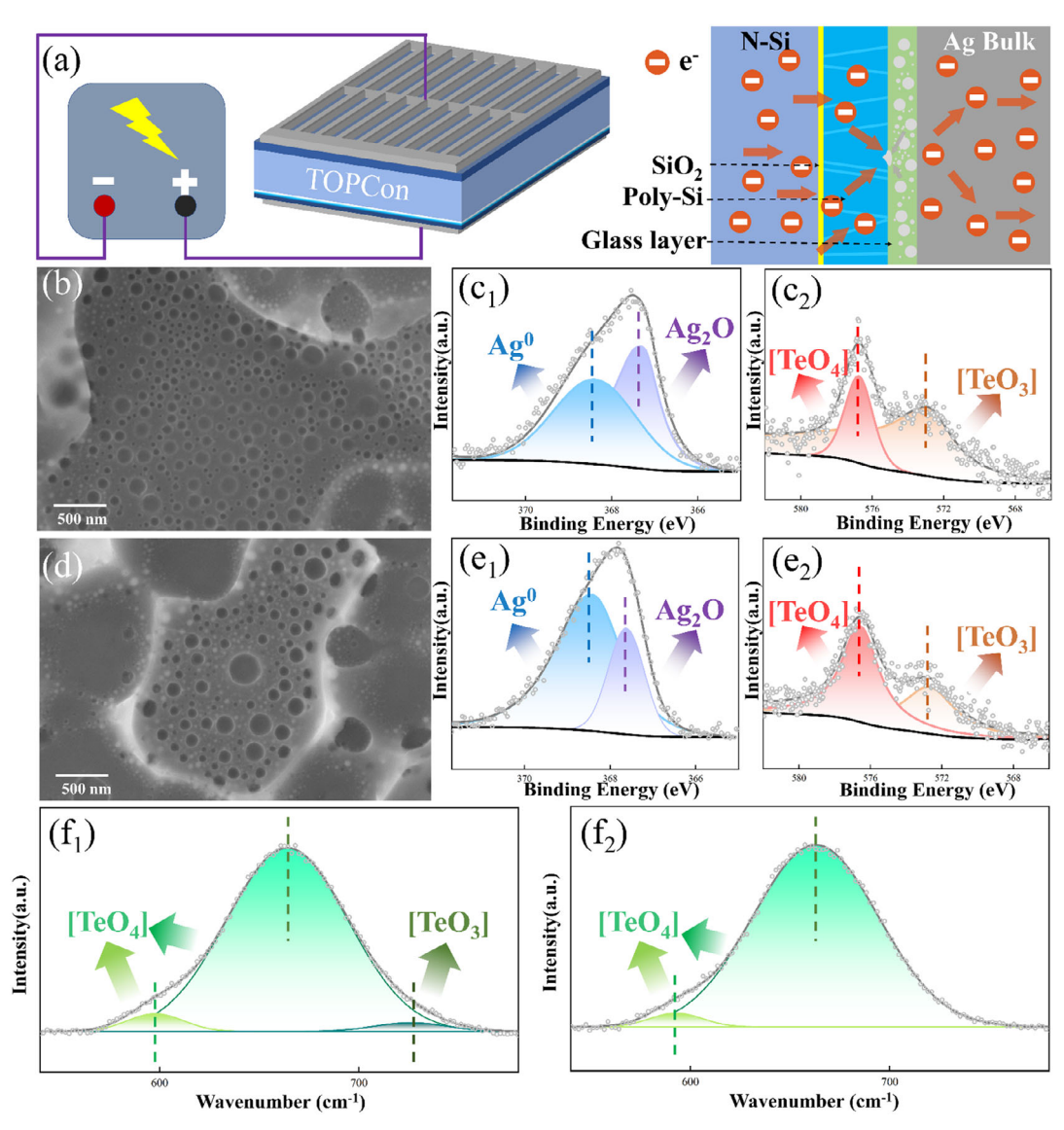


FIGURE 5 I (a) Schematic diagrams of LECO process and the change occurring in the contact area on the rear-side of the TOPCon solar cells during the LECO process; the SEM images of the contact area, after removing the Ag finger, on the rear-side of a TOPCon c-Si solar cell fabricated at 760°C before (b) and after (d) LECO; XPS results of corresponding samples before (c_{1-2}) and after (e_{1-2}) LECO, respectively; Raman results of corresponding samples before (f_1) and after (f_2) LECO, respectively.

in the glass layer exhibit superior conductivity, attracting more carriers (electronics) during LECO.

The XPS results of the sample corresponding to Figure 5b, shown in Figure $5c_{1-2}$, indicate that the Ag in the glass layer exists in the forms of Ag^0 and Ag_2O [25]. Meanwhile, TeO_3 and TeO_4 are identified as the primary Te oxidation states in the glass layer, consistent with the XPS results [26]. Furthermore, the XPS results of the sample corresponding to Figure 5d show an increase in the ratio of Ag to Ag_2O and a decrease in the ratio of TeO_3 to TeO_4 (as illustrated in Figure 5e and Table 1 [27].

The transformation of the glass structure was also confirmed by Raman spectroscopies. By peak fitting the Raman spectra before and after LECO, it can be observed that a peak corresponding to ${\rm TeO_3}$ exists at 727 cm⁻¹ before LECO (in Figure ${\rm 5f_1}$), but disappears after LECO (in Figure ${\rm 5f_2}$).

In our previous research, the impact of Ag on the structure of glass frit was thoroughly investigated. During the sintering process, Ag enters the glass network in the form of Ag_2O , causing the transformation of TeO_4 into TeO_3 [19b]. This mechanism can equally explain the changes observed during LECO. During the LECO process, a large number of electrons were flowing through the glass layer, reducing of Ag^+ within the glass layer to Ag colloids or forming of Ag crystallites. Concurrently, the decrease in Ag^+ concentration triggered a reversal in the glass layer, where TeO_3 reverts to TeO_4 . This growth process of Ag could be represented by the following equation:

$$Ag^+ + e^- \stackrel{LECO}{\rightarrow} Ag$$
 (8)

In addition, etching SiN_x layer and providing growth sites on the poly-Si is essential for directional growth of Ag crystallites on poly-Si [28]. Therefore, when the sintering temperature was

TABLE 1 | Semi-quantitative analysis of XPS spectra for Ag and Te before and after LECO.

Sample		Binding Energy (eV)	FWHM (eV)	Area (CPS.eV)	Atomic (%)
Before LECO	Ag 3d _{5/2} Scan A	368.39	2.24	2964.39	50.53
	Ag 3d _{5/2} Scan B	367.29	1.30	2902.92	49.47
After LECO	Ag 3d _{5/2} Scan A	368.40	1.83	4942.29	72.32
	Ag 3d _{5/2} Scan B	367.62	0.99	1892.25	27.68
Before LECO	Te3d Scan A	572.90	5.51	7593.46	78.63
	Te3d Scan B	576.74	1.85	2060.97	21.37
After LECO	Te3d Scan A	572.69	3.63	3834.13	43.45
	Te3d Scan B	576.52	2.53	4982.65	56.55

reduced to 710°C, due to insufficient etching of the SiN_x layer, even after LECO treatment, the ρ_c could not be reduced to an appropriate level (in Table S2, Supporting Information). This resulted in the 710°C cell with lower PCE than 760°C cell (in Table S1, Supporting Information).

Overall, the emergence of LECO represents a milestone advancement in metallization processes. LECO can simultaneously enhance the Ag-Si contact on both the front and rear side of TOPCon cells, albeit through different mechanisms and structures. Through detailed research, we revealed the dual impact, the current's thermal effect and electrochemical reduction reaction, of LECO on the Ag-Si contact on the rear of the TOPCon c-Si solar cells. Due to the interaction between the n-type poly-Si on the rear side and transportation of high-concentration electrons induced by laser, the Ag+ in the glass layer were reduced to Ago and form Ag colloids and crystallites that came into direct contact with the poly-Si. Compared to the uncontrollable Ag crystallites formed through hightemperature sintering, LECO enables the regulation of Ag crystallites growth. It allows for a finer balance between passivation and contact within the devices. Furthermore, by analyzing the ρ_c and microstructure of Ag-Si contacts formed at different temperatures, it can be observed that the ρ_c is lower when Ag crystallites are in direct contact. The results after LECO indicate that good contact performance can be achieved with smaller Ag crystallite and smaller effective contact areas.

4 | Conclusion

In conclusion, this work elucidated the mechanism through which LECO's electrochemical reduction promotes the growth of silver microcrystals. TOPCon solar cells featuring various structures of the rear Ag–Si contact interface were fabricated by modulating the sintering temperature and utilizing the LECO process. It was discovered that the formation of Ag crystallites plays a crucial role in decreasing the rear Ag-Si ρ_c in the rear contact. By lowering the sintering temperature, the etching of the rear SiN $_x$ layer by the glass frit was mitigated, thus reducing the carrier recombination at Ag–Si contact interface. However, it also hindered the formation of Ag crystallites at the contact interface, leading to an increase in ρ_c . The LECO process reduced Ag $^+$ in the glass layer to form Ag crystallites in direct contact with poly-Si and Ag nanoparticles within the glass

layer, which decreases the ρ_c . This work not only provides new insights into the construction of high-quality Ag–Si contacts but also elucidated the mechanism of action of LECO on the n-type side, which is of great significance for further optimizing the performance of TOPCon solar cells. Furthermore, by considering the optimization of glass composition and Ag powder structure, the etching of the passivation layer and the solubility of Ag in the glass layer could be better controlled. Combined with the formation of localized high-quality contacts through the LECO process, the PCE of the devices could be further enhanced.

Acknowledgments

The author would thank the support of the Soft Science Research Project of Guangdong Province (Grant No. 2017B030301013), and Guangdong Innovative Team Program (Grant No. 2013N080).

Conflicts of Interest

The authors declare no conflicts of interest.

Data Availability Statement

The data that support the findings of this study are available from the corresponding author upon reasonable request.

References

- 1. S. Chu and A. Majumdar, Nature 488 (2012): 294-303.
- 2. T. Kirchartz and U. Rau, $Advanced\ Energy\ Materials\ 8\ (\ 2018):\ 1703385.$
- 3. T. Nunoi, N. Nishimura, T. Nammori, H. Sawai, and A. Suzuki, *Japanese Journal of Applied Physics* 19 (1980): 67–70.
- 4. N. Chen and A. Ebong, Solar Energy Materials and Solar Cells 146 (2016): 107–113.
- 5. A. W. Blakers, A. Wang, A. M. Milne, J. Zhao, and M. A. Green, *Applied Physics Letters* 55 (1989): 1363–1365.
- 6. M. A. Green, E. D. Dunlop, M. Yoshita, et al., *Progress in Photovoltaics: Research and Applications* 32 (2024): 425–441.
- 7. F. Feldmann, M. Bivour, C. Reichel, M. Hermle, and S. W. Glunz, *Solar Energy Materials and Solar Cells* 120 (2014): 270–274.
- 8. T. Fellmeth, H. Höffler, S. Mack, et al., *Progress in Photovoltaics: Research and Applications* 30 (2022): 1393–1399.
- 9. (a) Y. Fan, S. Zou, Y. Zeng, et al., Solar RRL 8 (2024): 2400268. (b) Q. Wang, K. Guo, S. Gu, W. Huang, W. Wu, and J. Ding, Progress in Photovoltaics: Research and Applications 33 (2024): 294–308.

- (c) X. Wu, X. Wang, W. Yang, et al., Solar Energy Materials and Solar Cells 271 (2024): 112846. (d) R. Zhou, Y. Li, Z. Zhang, et al., Small 21 (2024): 2409628. (e) H. Höffler, F. Simon, E. Krassowski, and J. Greulich, "Siliconpv 2022, the 12th International Conference on Crystalline Silicon Photovoltaics," AIP Conference Proceedings 2826 (2023): 010001.
- 10. (a) G. K. Reeves and H. B. Harrison, *Electron Device Letters* 3 (1982): 111–113. (b) S. Grover, S. Sahu, P. Zhang, K. O. Davis, and S. K. Kurinec, in *2007 IEEE International Conference on Microelectronic Test Structures, Proceedings* (2020), 15–20.
- 11. K.-K. Hong, S.-B. Cho, J. S. You, J.-W. Jeong, S.-M. Bea, and J.-Y. Huh, Solar Energy Materials and Solar Cells 93 (2009): 898–904.
- 12. (a) T. C. Nason, L. You, and T. M. Lu, *Journal of Applied Physics* 72 (1992): 466–470. (b) M.-I. Jeong, S.-E. Park, D.-H. Kim, et al., *Journal of the Electrochemical Society* 157 (2010): H425.
- 13. H.-K. Kim, M. S. Kim, J.-W. Park, and W. J. Cho, Journal of the Electrochemical Society 154 (2007): J73.
- 14. (a) B. Feng, Y. Liu, W. Chen, G. Xing, X. Chen, and X. Du, *Solar Energy Materials and Solar Cells* 257 (2023): 112381. (b) W. Wu, C. Chan, M. Lewittes, L. Zhang, and K. Roelofs, *Energy Procedia* 92 (2016): 984–989.
- 15. I. B. Cooper, K. Tate, J. S. Renshaw, et al., *IEEE Journal of Photovoltaics* 4 (2014): 134–141.
- 16. (a) E. Cabrera, S. Olibet, J. Glatz-Reichenbach, R. Kopecek, D. Reinke, and G. Schubert, *Journal of Applied Physics* 110 (2011): 114511. (b) M. S. Jeong, S. H. Lee, S. Choi, et al., *ACS Applied Energy Materials* 6 (2023): 11983–11992. (c) M. I. Jeong, S. E. Park, D. H. Kim, et al., *Journal of the Electrochemical Society* 157 (2010): H934–H936. (d) W. Li, T. Wu, R. Jiao, et al., *Colloids and Surfaces A: Physicochemical and Engineering Aspects* 466 (2015): 132–137.
- 17. L. Wan, C. Zhang, K. Ge, et al., Advanced Energy Materials 10 (2020): 2070071.
- 18. J. Zhou, J. Zhang, and B. Lv, Solar Energy Materials and Solar Cells 259 (2023): 112439.
- 19. (a) H. Wang, S. Ma, M. Zhang, F. Lan, H. Wang, and J. Bai, *Journal of Materials Science: Materials in Electronics* 28 (2017): 11934–11949. (b) R. Zhou, Y. Li, W. Tan, Y. Lin, and F. Pan, *Solar RRL* 8 (2024): 2400299.
- 20. J. D. Fields, M. I. Ahmad, V. L. Pool, et al., *Nature Communications* 7 (2016): 11143.
- 21. M. Hörteis, T. Gutberlet, A. Reller, and S. W. Glunz, *Advanced Functional Materials* 20 (2010): 476–484.
- 22. B.-M. Chung, S.-B. Cho, J.-W. Chun, Y.-S. Kim, K. Okamoto, and J.-Y. Huh, *Electrochim Acta* 106 (2013): 333–341.
- 23. Y.-J. Chen, M.-J. Zhang, S. Yuan, et al., *Nano Energy* 36 (2017): 303–312.
- 24. R. F. Pierret and P. Hall, (1996). Semiconductor Device Fundamentals: United States Edition.
- 25. (a) H. Wang, J. Li, M. Zhou, et al., *Journal of Industrial and Engineering Chemistry* 30 (2015): 64–70. (b) A. M. Ferraria, A. P. Carapeto, and A. M. Botelho do Rego, *Vacuum* 86 (2012): 1988–1991.
- 26. (a) A. Bachvarova-Nedelcheva and R. Iordanova, *Comptes Rendus de L'Academie Bulgare des Sciences* 72 (2019): 1326–1335. (b) Y. Ma, J. Lin, S. Qin, L. Zhu, B. Li, and S. Lei, *Journal of Electronic Materials* 41 (2012): 646–650.
- 27. (a) A. Qin, Y. Fang, P. Tao, J. Zhang, and C. Su, *Inorganic Chemistry* 46 (2007): 7403–7409. (b) R. F. Cuevas, A. M. d. Paula, C. L. Cesar, L. C. Barbosa, and O. L. Alves, *Quimica Nova* 21 (1998): 361–364.
- 28. S. Choi, S. Cho, J. Lee, D.-Y. Jeong, and H. Kim, *Metals and Materials International* 21 (2015): 686–691.

Supporting Information

Additional supporting information can be found online in the Supporting Information section.